Trapped-Particle Instability Leading to Bursting in Stimulated Raman Scattering Simulations

S. Brunner*
Centre de Recherches en Physique des Plasmas, Association EURATOM-Confédération Suisse, EPFL, 1015 Lausanne, Switzerland

E. J. Valeo
Princeton Plasma Physics Laboratory, P.O. Box 451, Princeton, New Jersey 08543, USA–0451
(Received 26 October 2001; published 29 September 2004)

Nonlinear, kinetic simulations of stimulated Raman scattering (SRS) under laser-fusion conditions present a bursting behavior. Different explanations for this regime have been given in previous studies: saturation of SRS by increased nonlinear Landau damping [K. Estabrook *et al.*, Phys. Fluids B **1**, 1282 (1989)], and detuning due to the nonlinear frequency shift of the plasma wave [H. X. Vu *et al.*, Phys. Rev. Lett. **86**, 4306 (2001)]. Another mechanism, also assigning a key role to the trapped electrons is proposed here: the breakup of the plasma wave through the trapped-particle instability.

DOI: 10.1103/PhysRevLett.93.145003 PACS numbers: 52.35.Mw, 52.38.Bv, 52.65.Ff

A more thorough understanding of the dynamics of parametric instabilities is essential in order to improve the existing tools used for designing laser-fusion systems [1]. Stimulated Brillouin scattering (SBS) and stimulated Raman scattering (SRS) are the basic two such instabilities affecting the laser beam, respectively, involving the scattering off of ion-acoustic waves (IAWs) and electron plasma waves (EPWs). In the following, we shall essentially address issues involving the nonlinear evolution of SRS.

The bursting behavior of SRS appears as a common characteristic of different nonlinear, kinetic simulations [2,3]: Instead of reaching a steady state, with constant intensity of the reflected light, SRS presents an ongoing dynamical evolution, building up and breaking down in cycles. In these previous studies, different mechanisms have been suggested for this intermittence. The nonlinear wave-particle interaction has, however, always been identified as playing a key role: Estabrook, Kruer, and Haines [2] tentatively propose that SRS saturates as a result of increased nonlinear Landau damping, due to hot electrons generated through the trapping process, while Vu, DuBois, and Bezzerides [3] more recently interpreted their results by proposing that trapped particles lead to a significant nonlinear shift in the EPW frequency, which then detunes the parametric instability. On the basis of new simulations, a third possible mechanism for explaining the pulsating of SRS is presented in this Letter, also assigning an essential role to trapped electrons: The breakup of the EPW through a secondary instability, the so-called trapped-particle instability (TPI), first described by Kruer, Dawson, and Sudan [4,5].

The results are based on a spatially one-dimensional model with open boundaries, which represents the laser-plasma interaction along the beam. The Vlasov equation for both electrons and ions is solved numerically in the phase space (x, v_x)—x and v_x are, respectively, the position and velocity along the laser beam—by applying an Eulerian scheme [6], which evolves the particle distributions on a fixed Cartesian mesh in phase space. In this way, the essential kinetic effect, i.e., the nonlinear trapping of particles by the longitudinal waves in the plasma (EPWs and IAWs), is taken into account. The transverse motion is described in the cold fluid approximation. The physical parameters are inspired by conditions relevant to the National Ignition Facility [1]. The initial electron and ion temperatures are thus chosen $T_e = 1.5$ and $T_i = 0.1$ keV, and the density is assumed to be 10% of the critical density at the considered laser wavelength in vacuum $\lambda_0^{\text{vac}} = 0.351\ \mu$m. The initial distributions are assumed Maxwellian. By solving the matching condition equations for backward SRS [7], one obtains $(\omega_0/\omega_p = 3.162, k_0\lambda_D = 0.162)$, $(\omega_s/\omega_p = 2.065, k_s\lambda_D = -0.098)$, and $(\omega_e/\omega_p = 1.097, k_e\lambda_D = 0.260)$ for the frequencies and wave numbers of the incident light, scattered light, and EPW, respectively. Here ω_p is the plasma frequency and λ_D is the Debye length. The system length is taken $L = 4000\lambda_D = 110\lambda_0^{\text{vac}}$. Simulations were carried out for a set of incoming laser intensities in the range $I_0 = 1.0 \times 10^{14} - 1.6 \times 10^{15}\ \text{W cm}^{-2}$.

The particular case of incoming laser intensity $I_0 = 4 \times 10^{14}\ \text{W cm}^{-2}$ will now be considered in detail. The reflectivity as a function of time is shown in Fig. 1(a) for the whole simulation, which lasts $1.5 \times 10^4 \omega_p^{-1}$. The

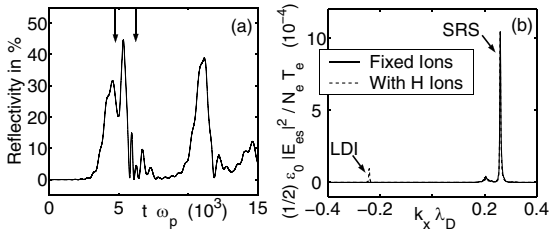

FIG. 1. (a) Backward SRS reflectivity as a function of time. (b) Energy k spectrum with and without ion dynamics.

evolution of SRS is clearly an ongoing dynamic process: The intensity of the reflected light successively increases, peaks, and then drops sharply to relatively low levels. This cycle repeats itself with a certain regularity, the recovery period in this case being approximately $5 \times 10^3 - 6 \times 10^3 \omega_p^{-1}$. The average reflectivity over the whole simulation is $\langle R \rangle = 8.6\%$, while peak values are up to 5 times larger.

To demonstrate that ion dynamics only play a minor role in saturating SRS in this case, the simulation was carried out considering proton ions so as to maximize the possible ion response. The same simulation was then also repeated with fixed ions. As shown in Fig. 1(b), the k spectra for these two simulations are nearly equivalent, except for a minor peak related to the Langmuir decay instability (LDI) of the primary EPW, thus reflecting the very small role played by this saturation channel.

A view of what is occurring within the interaction region during the SRS cycles is given in Fig. 2, where the electrostatic field $E_{\mathrm{es},x}$ of the EPW is plotted as a function of position and time. Figure 2(a) is a low resolution plot, showing the envelope of the field over the full length L of the simulation, and for the time interval $3 \times 10^3 < t\omega_p < 9 \times 10^3$ corresponding to the first burst. Note the positions in Fig. 2(a) of antennas 1 and 2, emitting, respectively, the laser light and seed for the scattered light ($I_s^{\mathrm{seed}} = 10^{-4} I_0$), in lieu of the electromagnetic thermal noise fluctuations, not contained as such in our model.

Considering this first SRS cycle, the field $E_{\mathrm{es},x}$ progressively builds up until time $t\omega_p \simeq 5 \times 10^3$, in conjunction with increasing reflectivity [Fig. 1(a)]. During this growth stage, the EPW remains a coherent field, with the constant phase characteristics traveling at the phase velocity $v_{\phi,e} = \omega_e / k_e = 4.2 v_{\mathrm{th},e}$. Only a slight, periodic modulation of the field's envelope is to be noted. In particular, as shown clearly in Fig. 3(a) for $t\omega_p = 4.8 \times 10^3$, the essentially monochromatic wave enables trapping of the resonant electrons. After time $t\omega_p \simeq 5 \times 10^3$, the EPW starts to breakup beyond $x = 2.5 \times 10^3 \lambda_D$, this breakup ultimately expanding to the entire field, which disintegrates into individual wave packets that drift off at the group velocity $v_{g,e} = 3 v_{\mathrm{th},e}^2 (k_e/\omega_e) = 0.71 v_{\mathrm{th},e}$. This event occurs simultaneously with the first drop of reflectivity in Fig. 1(a). At this point, the system undergoes a less coherent regime, reflected by the more chaotic particle orbits in phase space [see Fig. 3(b)]. Following its disintegration, the remains of the EPW have essentially damped out and convected out of the interaction zone after a time interval of $\sim 4 \times 10^3 \omega_p^{-1}$. Once the system has reached this more quiescent state, SRS is able to recover, leading to the next burst in reflectivity.

A key observation was made when repeating the same simulation, but artificially turning off the self-consistent ponderomotive drive at time $t\omega_p = 4.6 \times 10^3$, and noticing that the EPW evolved in essentially the same way. One can therefore conclude that the breakup is the result of an instability affecting the EPW itself, independent of the three-wave interaction of the parametric instability.

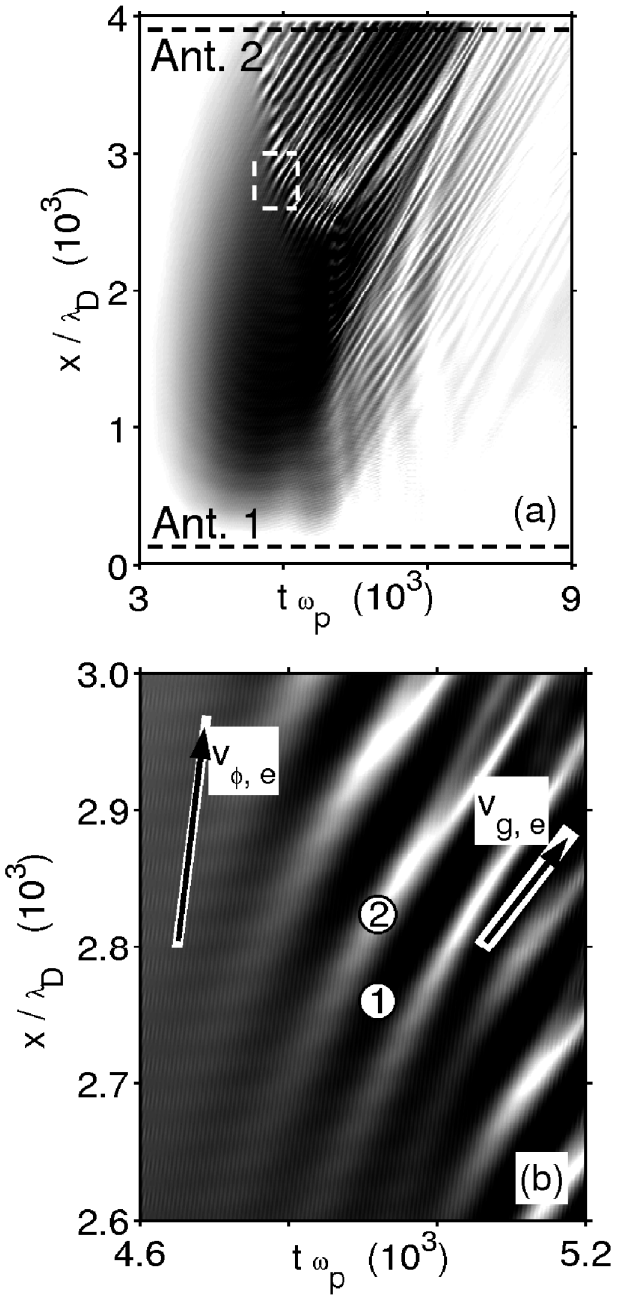

FIG. 2. (a) Envelope of the electrostatic field during the first cycle of SRS. Having reached a finite amplitude, the wave breaks up in packets, drifting off at the group velocity $v_{g,e}$. (b) Close-up view of the breakup [dash-bordered region in (a)]. Visible is the spatial modulation leading to the breakup. Points one and two correspond, respectively, to a maximum and minimum of the modulation along a constant phase characteristic traveling at the phase velocity $v_{\phi,e}$.

A close-up view of the breakup is given by Fig. 2(b), corresponding to the dash-bordered region in Fig. 2(a). It is apparent from this figure, that the modulation of the

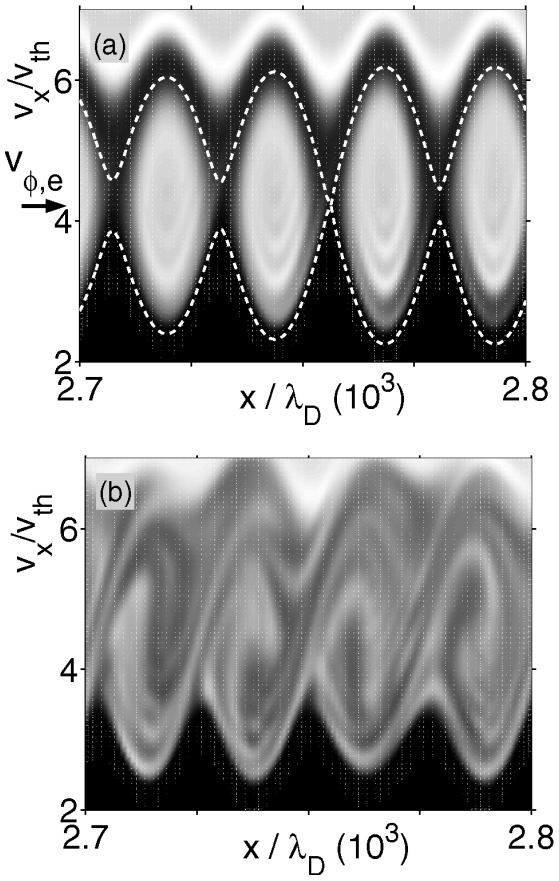

FIG. 3. Electron distribution at time (a) $t\omega_p = 4.8 \times 10^3$ and (b) $t\omega_p = 6.2 \times 10^3$ [times pointed out in Fig. 1(a)], in a limited region of phase space (x, v_x), corresponding to approximately four wavelengths of the main plasma mode. The separatrix of the trapping region is represented by dashed lines in (a).

initially coherent field provides the seed to the instability. The origin of the modulation can be identified by considering the electron velocity distribution function, averaged over one wavelength $\lambda_e = 2\pi/k_e$, at two different points along a same phase characteristic, one corresponding to a maximum, the other to a minimum in the modulation. Two such points have been chosen in Fig. 2(b), and the corresponding averaged distributions are given in Fig. 4. Obviously, the distribution inverts itself at the resonant phase velocity $v_{\phi,e}$ when going from a maximum to a minimum of the modulation, reflecting different bounce phases of the trapped electrons. The time separating two such points thus enables us to estimate the bounce period $\tau_b \simeq 42\omega_p^{-1}$. The wavelength λ_{mod} of the spatial modulation is directly related to τ_b, by the relation $\lambda_{\mathrm{mod}} \simeq v_{\phi,e}\tau_b \simeq 175\lambda_D$.

The spatial modulation naturally translates itself in Fourier space by the presence of sidebands $k_e \pm \Delta k_{\mathrm{mod}}$ to the main plasma mode k_e, where $\Delta k_{\mathrm{mod}} = 2\pi/\lambda_{\mathrm{mod}}$. The time evolution of these sidebands are plotted in Fig. 5(a), showing exponential growth in an interval of

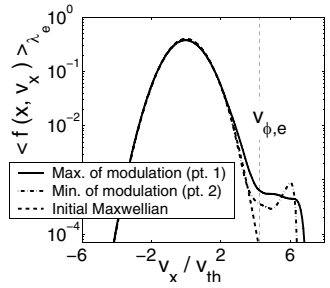

FIG. 4. Velocity distribution averaged in space over one wavelength λ_e. Going from a maximum to a minimum of the field modulation [points 1 and 2 in Fig. 2(b), respectively], the distribution systematically inverts itself around the phase velocity $v_{\phi,e}$.

a few τ_b around $t\omega_p = 5 \times 10^3$, characteristic of the linear stage of an instability. From these curves, the growth rate of sidebands $k_e \pm \Delta k_{\mathrm{mod}}$ are estimated to be $\gamma = 1.3 \times 10^{-2}\omega_p$ and $\gamma = 4.2 \times 10^{-3}\omega_p$, respectively.

The observations made by studying our simulation results of SRS bursting may thus be summarized as follows: (1) The turn-off of SRS reflectivity is the result of a secondary instability, affecting the EPW itself. (2) This instability involves sidebands of the initial large amplitude EPW. (3) The dynamics of trapped particles seem to play an essential role in the instability process. Considering these properties, the mechanism of the TPI appears as a logical explanation for the observed event. Indeed, given a large amplitude EPW, the TPI involves sidebands driven by the electrons trapped in the troughs of the main mode.

In their reduced model for the TPI, Kruer, Dawson, and Sudan [4] represent the electrons trapped within one potential well by a single, harmonically bound macroparticle. Implemented in this simple way, trapping is the only kinetic effect included in this model, which in all other respects is fluidlike. In particular, Landau damping of the EPW is neglected. In this framework, the dispersion relation for the TPI [Eq. (7), Ref. [4]] has three independent parameters: The wave number k_e of the principal plasma wave, the bounce-frequency ω_b, and the fraction f_t of trapped particles. To compare the solu-

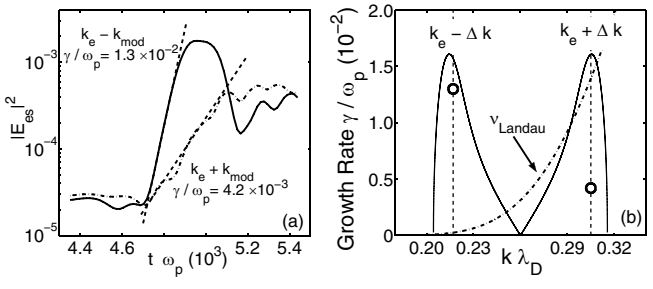

FIG. 5. (a) Time evolution of sidebands $k_e \pm \Delta k_{\mathrm{mod}}$. (b) Comparing growth rates γ of the sidebands (circles) with the solution to the dispersion relation for the TPI (full line).

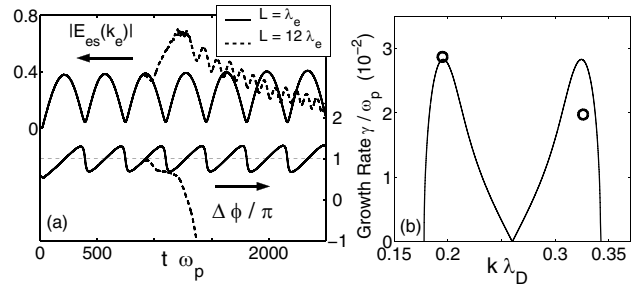

FIG. 6. Reduced simulation results. (a) Amplitude of $E_{\mathrm{es},x}$ in units $T/e\lambda_D$ (left scale), and dephasing $\Delta\phi$ with respect to external drive E_x^{ext} (right scale), for the $L = \lambda_e$ and $L = 12\lambda_e$ long systems. (b) Comparison of sideband growth rates in $L = 12\lambda_e$ system, with results from the TPI dispersion relation.

tion of this dispersion relation to the growth rates of the sidebands $k_e \pm \Delta k_{\mathrm{mod}}$ from our simulations, these parameters are thus given the values $k_e\lambda_D = 0.260$, $\omega_b = 2\pi/\tau_b = 0.15\omega_p$, and $f_t = 0.12\%$, f_t having been integrated from the distribution in Fig. 3(a). The corresponding result is shown in Fig. 5(b), and presents the typical, double-humped shape, symmetrical around the principal wave number k_e. The linear evolution of the simulation sidebands $k_e \pm \Delta k_{\mathrm{mod}}$ agrees well with the peaks of the dispersion relation solution, both in the values of the wave numbers and growth rates. The agreement is noteworthy considering the relative simplicity of the macroparticle model. The fact that the simulation growth rates are somewhat lower than predicted by the dispersion relation, especially for the upper sideband, can be assigned to Landau damping. This point is also illustrated in Fig. 5(b), where the linear Landau damping, increasing with $k\lambda_D$, has been added for comparison.

Further credibility to the essential role played by the TPI in the mechanism leading to the bursting of SRS is given by studying a reduced simulation system with fixed ions, periodic boundaries instead of open ones, and the resonant component of the self-consistent ponderomotive force replaced by an external drive $F_x^{\mathrm{ext}} = (-e)E_x^{\mathrm{ext}} = (-e)E_0\cos(k_e x - \omega_e t)$. The values ($\omega_e/\omega_p = 1.097$, $k_e\lambda_D = 0.260$) are chosen so as to reproduce the conditions of the full simulation. So as to shorten the time scale for illustrative purposes, the amplitude $E_0 = 8 \times 10^{-3} T/e\lambda_D$ of the drive was, however, chosen larger by a factor of 4 than the time averaged value from the full simulation. In a first run, the reduced system is taken just one wavelength long, $L = 2\pi/k_e$, so that no sidebands besides the harmonics of the main mode are allowed. This setup is similar to the one considered by Cohen and Kaufman [8]. In a second run, sideband effects are enabled by increasing the system to the arbitrary length $L = 12 \times 2\pi/k_e$.

In the single wavelength simulation, and as a result of the nonlinear frequency shift, the phase difference $\Delta\phi$ between the principal plasma wave $E_{\mathrm{es},x}$ and the drive E_x^{ext} oscillates around π, and its amplitude thus presents a periodic modulation in time [Fig. 6(a)]. This is similar to the result in Fig. 4 of Ref. [8]. In the multiple wavelength simulation, however, the harmonic modulation is rapidly interrupted, the phase lock-in with the drive is lost, and the main mode k_e depletes itself in a way comparable to the breakdown of reflectivity shown in Fig. 1. This depletion occurs in conjunction with the growth of sidebands, which, after comparison with the macroparticle model, can again be related to the TPI [Fig. 6(b)]. In this case, the simulation provided the parameter estimates $\omega_b = 0.20\omega_p$ and $f_t = 0.49\%$ for solving the TPI dispersion relation.

The other simulations performed at same density and temperatures but higher intensities up to $I_0 = 1.6 \times 10^{15}\ \mathrm{W\,cm^{-2}}$ all present similar bursting of SRS, and the observed sideband growth rates remain in good semiquantitative agreement with those predicted by the TPI dispersion relation. At even larger intensities however, a significant amount of LDI starts to be observed. Although dominant in our lower intensity computations, the TPI may not be the only possible process leading to the SRS pulsations. Indeed, as partly observed in our reduced simulations, other effects, such as detuning resulting from the nonlinear frequency shift of the plasma wave [3], may also contribute, either simultaneously, or in turns.

We wish to thank R. L. Berger for helpful discussions. This work was supported by the Lawrence Livermore National Laboratory under DOE Interoffice Work Order Number B344523, by the U.S. Department of Energy Contract No. DE–AC02–76–CHO–3073.

*Email address: stephan.brunner@epfl.ch

[1] J. Lindl, Phys. Plasmas **2**, 3933 (1995); J. Lindl *et al.*, Phys. Plasmas **11**, 339 (2004); S. E. Bodner *et al.*, Phys. Plasmas **5**, 1901 (1998).
[2] K. Estabrook, W. L. Kruer, and M. G. Haines, Phys. Fluids B **1**, 1282 (1989).
[3] H. X. Vu, D. F. DuBois, and B. Bezzerides, Phys. Rev. Lett. **86**, 4306 (2001).
[4] W. L. Kruer, J. M. Dawson, and R. N. Sudan, Phys. Rev. Lett. **23**, 838 (1969).
[5] D. A. Hartmann and C. F. Driscoll, Phys. Plasmas **8**, 3457 (2001).
[6] C. Z. Cheng and G. Knorr, J. Comput. Phys. **22**, 330 (1976); P. Bertrand *et al.*, Phys. Fluids B **2**, 1028 (1990).
[7] W. L. Kruer, *The Physics of Laser Plasma Interactions* (Addison-Wesley, New York, 1988).
[8] B. I. Cohen and A. N. Kaufman, Phys. Fluids **20**, 1113 (1977).